Journal of The Electrochemical Society, **151** (10) G697-G703 (2004)
0013-4651/2004/151(10)/G697/7/$7.00 © The Electrochemical Society, Inc.

Effect of NH_3 on Film Properties of MOCVD Tungsten Nitride from $Cl_4(CH_3CN)W(N^iPr)$

Omar J. Bchir,[a,*] Kee Chan Kim,[a] Timothy J. Anderson,[a,] Valentin Craciun,[b] Benjamin C. Brooks,[c] and Lisa McElwee-White[c]**

[a]*Department of Chemical Engineering, University of Florida, Gainesville, Florida 32611, USA*
[b]*Major Analytical Instrumentation Center, Department of Materials Science and Engineering, University of Florida, Gainesville, Florida 32611, USA*
[c]*Department of Chemistry, University of Florida, Gainesville, Florida 32611, USA*

Thin films of tungsten nitride were deposited from $Cl_4(CH_3CN)W(N^iPr)$ by metallorganic chemical vapor deposition (MOCVD) in the presence and absence of ammonia (NH_3) coreactant. Films were analyzed by X-ray diffraction, Auger electron spectroscopy, and X-ray photoelectron spectroscopy (XPS). Films grown with NH_3 had increased nitrogen levels and decreased carbon and oxygen levels relative to films grown without NH_3 over the entire deposition temperature range (450-700°C). Deposition with NH_3 at higher temperature (≥600°C) led to higher crystallinity. Binding energies from XPS measurements were consistent with the formation of WN_x (or WN_xC_y) and WO_3 in the films, regardless of whether NH_3 was present. The addition of NH_3 at lower deposition temperature increased film resistivity significantly.
 [DOI: 10.1149/1.1789412]

Manuscript submitted October 27, 2003; revised manuscript received March 13, 2004. This was Paper 2098 presented at the Paris, France, Meeting of the Society, April 27-May 2, 2003. Available electronically September 27, 2004.

The transition from aluminum to copper as the interconnect material for integrated circuits is due to copper's higher resistance to electromigration and its lower resistivity. Unfortunately, Cu is highly mobile in Si and SiO_2.[1] Migration of the metal following exposure of Si to copper can cause an increase in contact resistance, change in the barrier height, leaky p-n junctions, embrittlement of the contact layer, and destruction of electrical connections to the chip.[2] As a result, a high-quality diffusion barrier layer is essential to preventing Cu-Si interaction. This barrier should have minimal impact on the line and via resistance of each interconnect layer, minimum layer thickness, good conformality, low resistivity, an available low-temperature deposition method, and amorphous film structure.

Both tungsten nitride (WN_x) and tantalum nitride (TaN) appear to promise better copper barrier integrity at elevated temperatures than TiN, the typical barrier material in Al metallization schemes.[3-5] As an alternative Cu diffusion barrier, WN_x appears to have technological advantages over TaN. WN_x is known to be an effective barrier against Cu migration at temperatures below 750°C and Cu can be deposited by chemical vapor deposition (CVD) on WN_x with better adhesion properties than those obtained with TaN.[6,7] In addition, WN_x outperforms TaN as a liner material for seedless electrochemical deposition (ECD), as ECD Cu shows a higher nucleation density on and stronger adhesion to WN_x film layers.[8-10] Finally, WN_x is more easily planarized by chemical mechanical polishing (CMP) than TaN, thereby minimizing dishing of the neighboring Cu.[11,12]

Metallorganic chemical vapor deposition (MOCVD) of WN_x provides a promising approach to diffusion barriers for Cu metallization because it enables low-temperature deposition, minimal halide incorporation, good conformality, and negligible pitting of the underlying Cu line. The major challenge for MOCVD is minimizing contamination by carbon and oxygen from the precursor and solvent (when applicable). The presence of carbon and oxygen can improve barrier integrity at moderate levels but tends to increase film resistivity at higher concentrations, undermining the benefits gained from Cu metallization.[13]

Two metallorganic precursors, tungsten(0) hexacarbonyl [$W(CO)_6$] and tungsten(0) pentacarbonyl 1-methylbutylisonitrile [$W(CO)_5(C_5H_{11}NC)$], have been used with NH_3 as a coreactant to deposit films by MOCVD.[14,15] A single-source tungsten imido precursor, $(^tBuN)_2W(NH^tBu)_2$, has also been employed to deposit WN_x thin films by MOCVD.[16,17] In related work, a recent report demonstrated growth of WN_x by atomic layer deposition (ALD) using $(^tBuN)_2(Me_2N)_2W$ and NH_3 as reactants.[18] It is suggested that including NH_3 in the reactant stream leads to reduced levels of C and O incorporation. MOCVD involving NH_3 addition to a precursor with a preexisting W-N multiple bond, however, has yet to be examined. In this study, we report initial results for the addition of NH_3 as a coreactant gas during deposition of WN_x thin films from the tungsten imido precursor $Cl_4(CH_3CN)W(N^iPr)$. The effect of NH_3 addition on film composition, crystallinity, and bonding state is presented.

Experimental

Precursor synthesis and screening were carried out as reported previously.[19,20] The solid precursor was dissolved in benzonitrile solvent at a concentration of 7.5 mg/mL, loaded into a syringe and pumped into a nebulizer, which creates a mist of precursor-containing solvent droplets. Hydrogen (H_2) carrier gas conveys the droplets through a heated impinging jet and out of a showerhead to the substrates, which rest on a radio-frequency (rf) heated graphite susceptor inside the reactor. Experiments were conducted in a custom-built vertical quartz cold wall CVD reactor system. p-Type boron-doped Si(100) substrates with resistivity of 1-2 Ω cm were used for film growth.

The total carrier gas flow rate was fixed at 1000 sccm, with pure H_2 used for depositions without NH_3 and a H_2/NH_3 flow rate ratio of 999/1 used for the ammonia runs. The deposition temperature ranged from 450 to 700°C, and the pressure was fixed at 350 Torr. After growth, film crystallinity was analyzed by XRD using a Philips APD 3720, and composition was determined by Auger electron spectroscopy (AES) using a Perkin-Elmer PHI 660 scanning Auger multiprobe. X-ray photoelectron spectroscopy (XPS) data were collected with a Perkin-Elmer PHI 5100 ESCA system using a Mg anode X-ray source. The nominal sputter rate for AES was 100 Å/min, while that for XPS was 20 Å/min. Sputtering times for AES and XPS were adjusted to 2 and 10 min, respectively, to analyze films at roughly equal depths. The film density was estimated with X-ray reflectivity (XRR) using a Philips MRD X'Pert system, while the film roughness was analyzed by atomic force microscopy (AFM) using a Digital Instruments Nanoscope III.

* Electrochemical Society Student Member.
** Electrochemical Society Active Member.

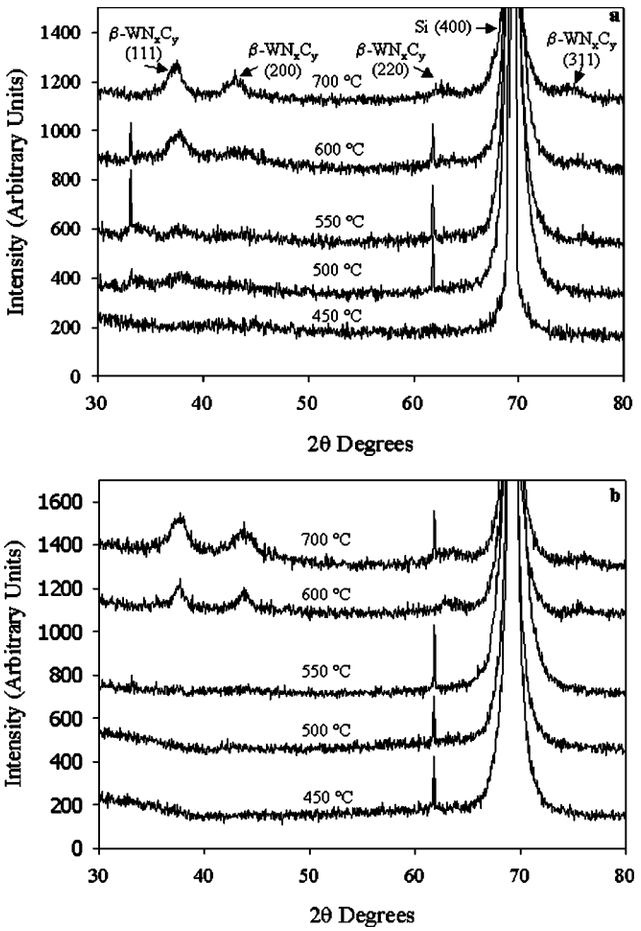

Figure 1. XRD spectra for films grown on Si(100) in a H_2 atmosphere (a) without NH_3 and (b) with NH_3.

Results and Discussion

Growth of WN_x films from the $Cl_4(CH_3CN)W(N^iPr)$ precursor was previously demonstrated.[20] Films deposited below 500°C had an amorphous structure, while those deposited at and above 500°C were polycrystalline. Film composition studies indicated that carbon contamination increased with deposition temperature, and that the films were low in nitrogen, with a maximum nitrogen content of 11 atom % at 500°C. Importantly, any Cl in the films was below the AES detection limit. The apparent activation energy for film growth from the precursor was determined to be 0.84 eV, while the growth rates varied from 10 to 27 Å/min throughout the deposition temperature range of 450 to 700°C. In addition, film resistivity ranged from 750 to 15000 μΩ cm, with the lowest value occurring in material deposited at 450°C.

Figure 1a illustrates the effect of deposition temperature on film crystallinity. The absence of WN_x peaks in the XRD spectra at 450°C suggests that films were X-ray amorphous. Crystallinity appeared in the films deposited above ~500°C, with the first peak emerging at $2\theta = 37.94$, consistent with polycrystalline β-W_2N(111) growth. This is in accord with a previous report that amorphous WN_x films transform into polycrystalline β-W_2N between 450 and 500°C.[21] As the deposition temperature increases to 600°C, the (111) peak sharpens and shifts to a lower 2θ value, consistent with β-WN_xC_y formation, in which N and C intermix on the face-centered cubic (fcc) W interstitial sublattice.[22] The (111) peak positions for the binary β-$WN_{0.5}$ and β-$WC_{0.5}$ phases are $2\theta = 37.74$ and 36.98, respectively, hence a peak between them suggests a ternary β-WN_xC_y phase.[23,24] Another broad peak at 44.42 2θ degrees also appears at this temperature, suggesting β-WN_xC_y (200) formation. Films deposited at 500 and 600°C displayed two additional peaks at 33.03 and 61.67° 2θ, representing Si(200) Kα and Si(400) Kβ radiation, respectively. Increasing the deposition temperature to 700°C results in further sharpening of the β-WN_xC_y (111) and (200) peaks; a shift to lower 2θ value for these peaks is consistent with decreasing x and increasing y in the β-WN_xC_y polycrystals. The emergence of two broad peaks at 63.00 and 75.82° 2θ at this temperature indicate β-WN_xC_y (220) and (311) formation. No XRD peaks consistent with graphite, metallic W, or WO_3 polycrystals were present in the spectra.

Deposition with NH_3 at 450°C resulted in deposition of an X-ray amorphous film, as had been observed without NH_3. Material grown with NH_3 at 500°C was also amorphous, in contrast to polycrystalline films grown without NH_3 at 500°C. This phenomenon may be due to surface site blocking and insufficient surface diffusion of NH_3 at lower deposition temperature. Addition of NH_3 resulted in similar spectra for films grown at 600 and 700°C, but with sharpened peaks (Fig. 1b) indicating enhanced grain growth relative to deposition without NH_3. In addition, the peaks at 63.00 and 75.82° 2θ appear for the 600°C deposition with NH_3, while they do not appear until 700°C for films deposited without NH_3. Carbon is reported to decrease grain size when added to refractory metal films.[25] Thus, the increase in polycrystal grain size is likely due to the decrease in carbon content (see Fig. 2c) accompanying NH_3 addition at these higher temperatures.

Figures 2a and b depict the impact of NH_3 addition on the concentration of tungsten and nitrogen, respectively, in the films. Addition of NH_3 dramatically increased the nitrogen levels over the entire deposition temperature range, as depicted in Fig. 2b. The concomitant decrease in W is attributed to the increased concentration of N in the films. The addition of ammonia increased the nitrogen content from 8 to 24 atom % for deposition at 450°C, and levels increased from 11 to 29 atom % at 500°C. As the deposition temperature increases to 600 and 700°C, N levels drop off. Metal nitride barriers typically show a decrease in N content with increasing deposition temperature, because higher temperatures impart more energy to the film lattice, inducing nitrogen to desorb as N_2 gas. Nitrogen loss from WN_x films has been reported at temperatures above 700°C, consistent with AES results in this range.[26] Similar experiments replacing NH_3 with N_2, an inert species at these temperatures, yielded poor film coverage and lower nitrogen levels than films deposited without a co-reactant.

Figure 2c depicts the change in carbon concentration with deposition temperature for films deposited with and without NH_3. Addition of NH_3 appears to have little impact on carbon content at the two lower deposition temperatures. This may reflect a change in the reaction kinetics of carbon removal processes between low and high temperature. Enhanced NH_3 decomposition at increased temperatures may improve production of gaseous carbon species (such as CH_4), which scavenge carbon from the film.

Figure 2d depicts the change in oxygen concentration with deposition temperature for films deposited with and without NH_3. Oxygen contamination results from post-growth exposure of the films to air, and high oxygen levels at low deposition temperatures are likely due to film porosity.[20] Oxygen content drops substantially for deposition without NH_3 between 450 and 500°C. Film crystallization at higher deposition temperature causes an increase in film density, which inhibits diffusion of oxygen into the films upon exposure to air. The ~12% drop in oxygen concentration for films deposited with NH_3 at 450°C relative to those without might suggest that addition of NH_3 leads to a denser amorphous film structure, which allows less oxygen indiffusion. However, this possibility was ruled out by density measurements (per XRR) of 8.3 and 8.6 g/cm^3, respectively, for films deposited at 450°C with and without NH_3. While these values are similar to those obtained for WN_x deposited

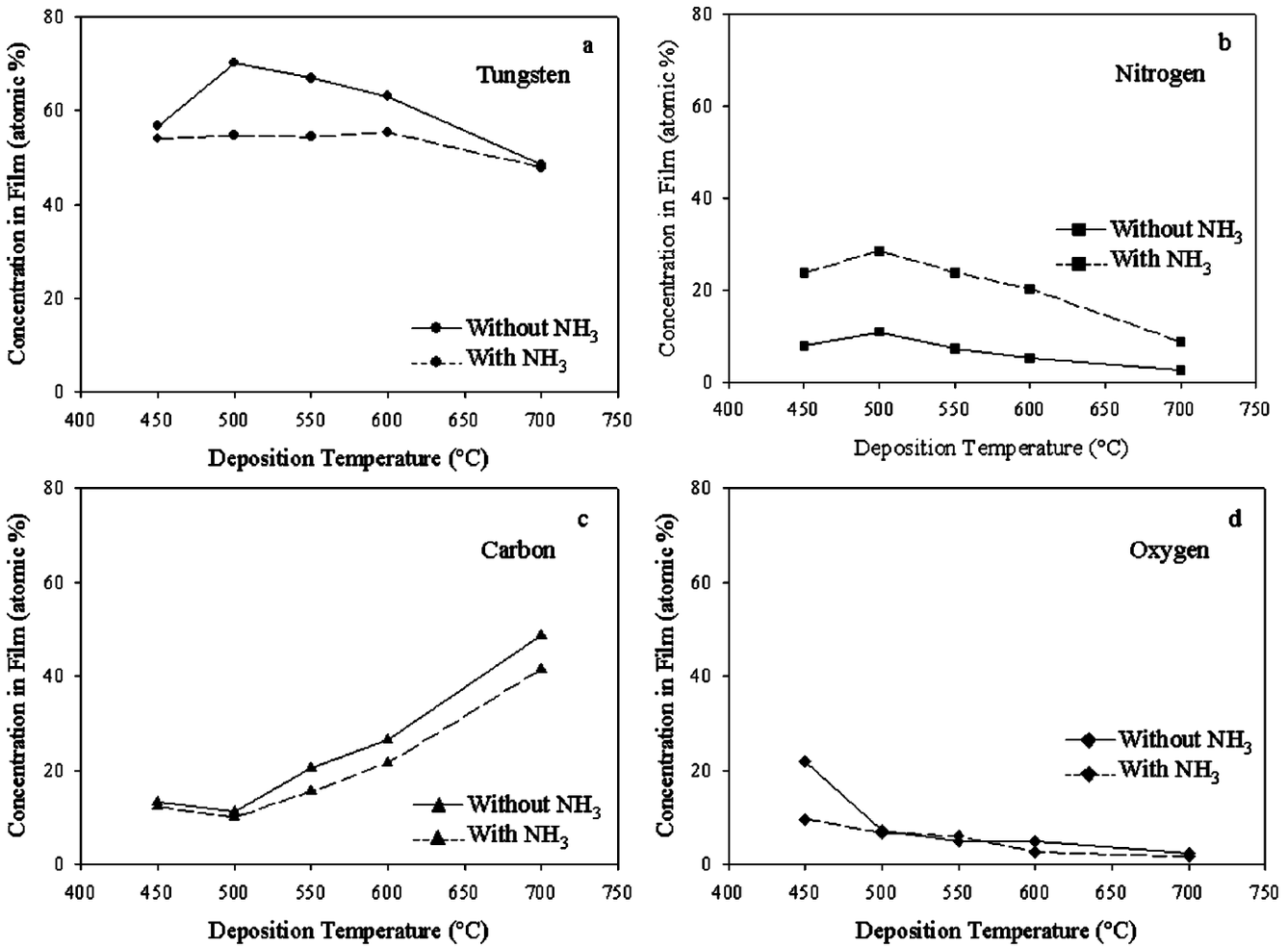

Figure 2. Variation of (a) tungsten, (b) nitrogen, (c) carbon, and (d) oxygen content in the films with deposition temperature. Data are estimated from AES spectra taken after 2 min sputter time.

with WF_6 and NH_3 at 450°C, they indicate that film density decreases with NH_3 addition.[27] Oxygen content was lower in these films, however, despite their lower density, suggesting that microstructure has greater impact than density on the film's resistance to post-growth oxygen incorporation. This is consistent with a previous report, which indicates that diffusion barrier performance depends more strongly on film microstructure than film density.[28]

As the deposition temperature increases above 500°C, the oxygen levels in both films decrease, becoming roughly equal near 2 atom % for deposition at 700°C. Similar oxygen concentrations at 700°C reflect the impact of polycrystal size and carbon contamination on oxygen diffusion. Films deposited without NH_3 have higher carbon content at 700°C, and this carbon is expected to stuff grain boundaries, preventing oxygen diffusion into the film. Films deposited with NH_3 have lower carbon contamination, but larger polycrystals, which resist oxygen migration.

XPS was used to determine binding energy (BE) and, therefore, bonding state for atoms in the deposited films. The W 4f, N 1s, C 1s, and O 1s photoelectron lines were used to examine the bonding states in the films for tungsten, nitrogen, carbon, and oxygen, respectively. The W 4f photoelectron line has two peaks (W $4f_{7/2}$ and W $4f_{5/2}$), while the N 1s, C 1s, and O 1s lines each have one. Literature BE values for potential compounds in the film are listed in Table I.

Table I. Literature binding energy values (eV).

Compound	W $4f_{7/2}$	W $4f_{5/2}$	N 1s	C 1s	O 1s	Ref.
Metallic W	31.2	33.4	—	—	—	29
WN_x	32.7-33.6	33.3-35.8	397.0-398.0	—	—	30-32
N at grain boundary	—	—	399.2-400.0	—	—	33, 34
$W(N, O)_x$	—	—	398.1-399.3	—	N/A	30
WO_3	35.5-36.7	37.6-37.8	—	—	530.1-531.6	30, 34, 35
WC_x	31.6-31.7	33.7-33.9	—	282.6-283.8	—	29, 36
Amorphous carbon	—	—	—	284.5-285.2	—	37, 38

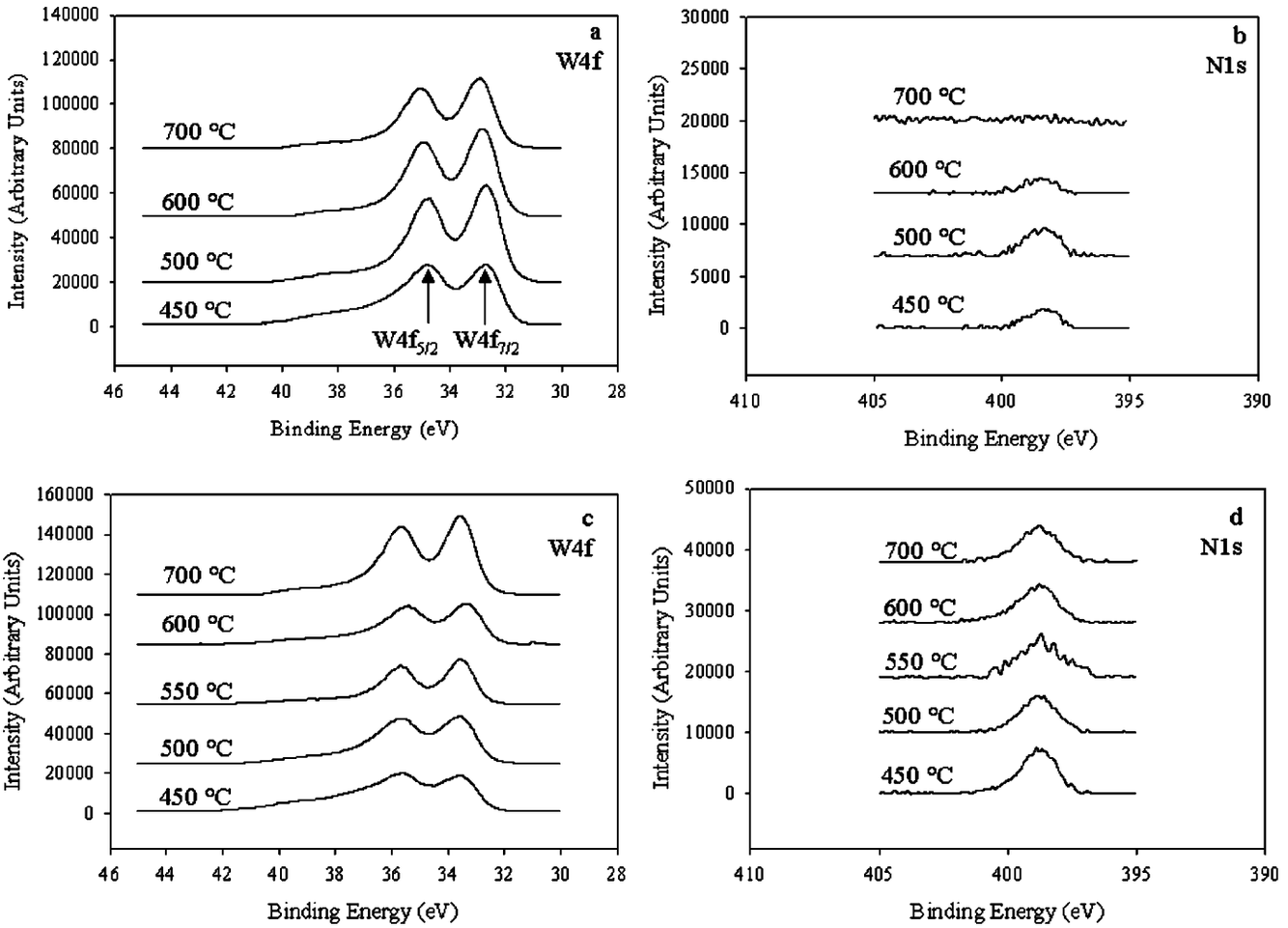

Figure 3. Variation of W 4f and N 1s binding energies with deposition temperature; (a and b) without NH_3, (c and d) with NH_3. Data are from XPS after 10 min sputter.

Figure 3a shows the variation of W 4f BE with deposition temperature for films deposited without NH_3. The principal W $4f_{7/2}$ and W $4f_{5/2}$ peaks for deposition at 450°C are at 32.6 and 34.7 eV, respectively, which are close to values reported for WN_x (Table I). These BE values are higher than metallic or carbidic W due to the ionic character of the W-N bond, and may represent W in the β-WN_xC_y bonding state.[31] Binding energy values for W in the β-WN_xC_y phase have not been reported, however, so a benchmark to confirm this bonding state is unavailable. Nitrogen atoms are more electronegative than W, which implies a $W^{\delta+}$-$N^{\delta-}$ type structure.[31] Ionic character in the bond causes a decrease in N 1s BE and an increase in W 4f BE relative to values for elemental W and N. Increasing the deposition temperature leads to a shift in W 4f BE values to 32.9 and 35.0 eV, which also correspond to WN_x. This small increase in BE may be due to charging, which is more likely for carbon-laden samples deposited at higher temperature. The shoulder at higher BE for the 450 and 500°C runs is likely due to the presence of WO_3. Peak deconvolution yields W $4f_{7/2}$ and W $4f_{5/2}$ BE values near 35.7 and 37.8 eV, which are near the WO_3 range displayed in Table I. Interestingly, the W 4f peak positions do not indicate the presence of any metallic or carbidic W. Hence, any carbon in the film is either bound in the β-WN_xC_y polycrystals or is at the grain boundary in amorphous form.

Figure 3b shows the variation of N 1s BE with deposition temperature for these same films. The N 1s peaks are centered near 398.3 eV, which is slightly higher than previous values reported for WN_x (Table I). While these peaks likely represent WN_x, the presence of tungsten oxynitride ($W(N, O)_x$), which has reported BE values as low as 398.1 eV (Table I), cannot be ruled out. Due to their similar lattice structures, the XRD pattern for $W(N, O)_{1.33}$ overlaps exactly with WN_x, and the presence of oxygen is evident from AES.[23,39] Alternatively, the upward shift in N 1s BE may represent an attractive N-C interaction on the interstitial sublattice of W in the β-WN_xC_y bonding state. An attractive N-C interaction on the fcc Nb and fcc Ti interstitial sublattices has been reported.[40]

Nitrogen atoms in WN_x are typically found either at octahedral interstitial sites within the crystal lattice or at the grain boundaries. The lack of a second N 1s peak above 399 eV suggests that all nitrogen is interstitial, with none present at the grain boundaries of the film. A single N 1s peak at all temperatures also indicates that nitrogen is bonded similarly at all temperatures, regardless of film crystallinity. Thus the amorphous films deposited at lower temperatures are likely to contain β-WN_xC_y, but in either unit cell or nanocrystalline size, both of which are invisible to XRD. The crystallite size increases with deposition temperature, with polycrystals becoming visible to XRD at 600 and 500°C for films deposited with and without NH_3, respectively.

The N 1s peak intensity increases from 450 to 500°C, which is consistent with AES results indicating higher nitrogen levels at 500°C. However, the intensity drops at 600°C, and then disappears into the background noise at 700°C. The disappearance of the N 1s peak contrasts with AES results for films grown at 700°C, which

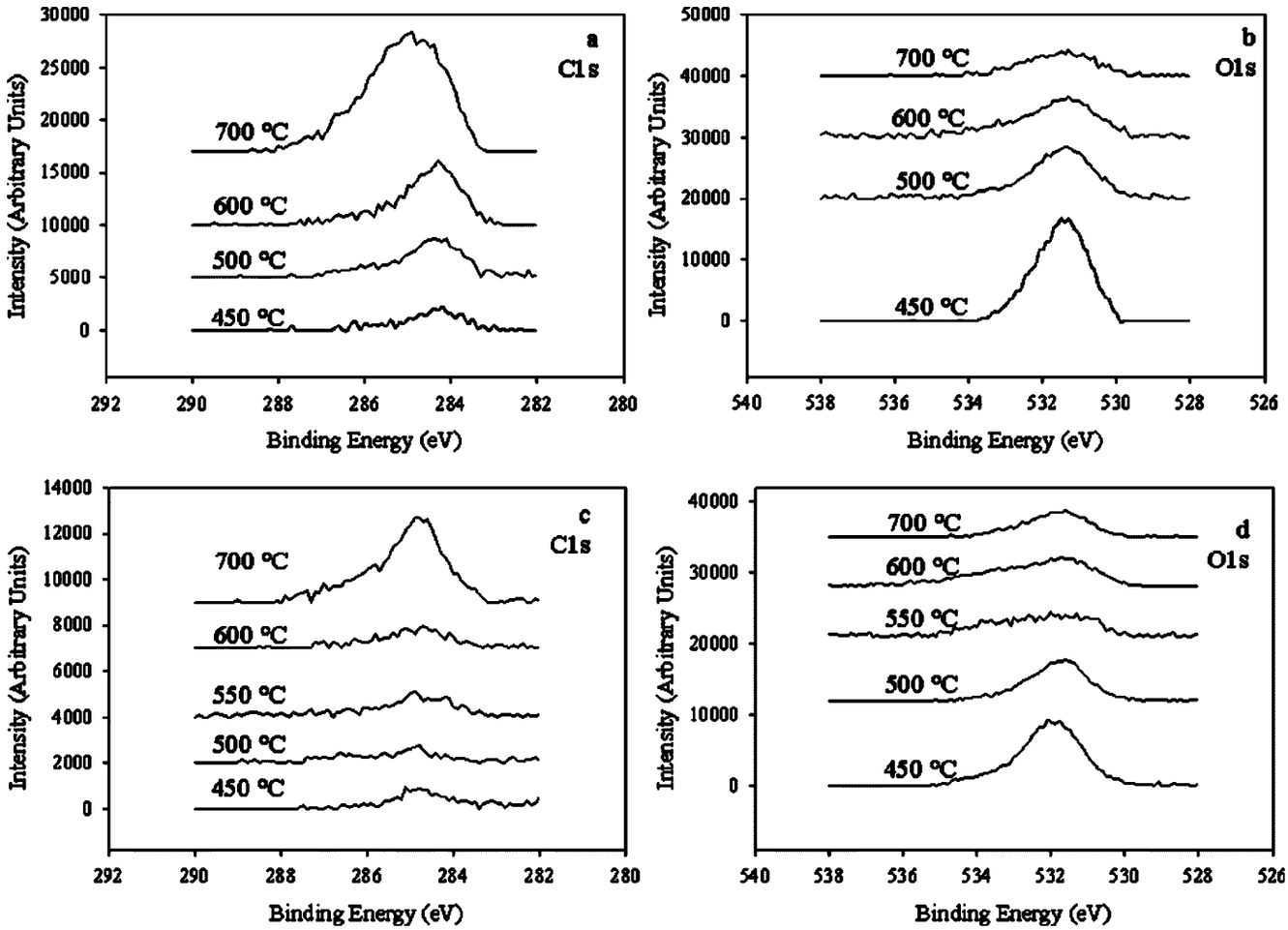

Figure 4. Variation of C 1s and O 1s binding energies with deposition temperature: (a and b) without NH_3, (c and d) with NH_3. Data are from XPS after 10 min sputter.

indicate that some nitrogen remains in the films. This discrepancy is possibly a result of large shifts in XPS sensitivity for nitrogen in compound materials, as have been reported.[41]

Figure 3c shows the effect of NH_3 addition on the W 4f binding energies. The principal W $4f_{7/2}$ and W $4f_{5/2}$ peaks for 450°C are at 33.6 and 35.6 eV, respectively, corresponding to the upper limit for WN_x (Table I). Again, this upward shift may be due in part to an attractive N-C interaction on the interstitial sublattice of W in the β-WN_xC_y bonding state. Although these BE values are stable over the entire temperature range, they are shifted to ~1 eV higher relative to films deposited without NH_3. This shift is due in part to increased nitrogen content in the films, which suggests greater occupancy of N sites relative to films depicted in Fig. 3a, and therefore more complete W-N bonding. Higher numbers of W-N bonds raise the partial positive charge at W and thereby increase the W 4f BE. In addition, some sample charging may occur, which would also cause an increase in BE. Like the films deposited without NH_3, a W 4f shoulder was observed for films deposited at lower temperatures, indicating the presence of WO_3.

Figure 3d shows the variation of N 1s BE with deposition temperature for films deposited with NH_3. The N 1s peaks are steady over the entire temperature range, and are centered around 398.8 eV, above the reported range for WN_x values (see Table I). This increase in N 1s BE is unusual, considering the increased W-N bonding that should occur for higher N content, and may be attributed to sample charging. Again, the upward shift in N 1s BE may also be due in part to an attractive N-C interaction on the interstitial sublattice of W in the β-WN_xC_y bonding state. In addition to BE, we note that the N 1s peaks endure through the entire temperature range for films deposited with NH_3. Although nitrogen content does drop for these films above 500°C, AES results in Fig. 2b indicate a substantial increase in nitrogen for these films relative to those grown without NH_3. This is consistent with competition between increased rates of nitrogen release from the film into the gas phase and higher reactivity of NH_3 with the growing film at higher temperatures.

Figure 4a shows the variation of the C 1s line with deposition temperature for films deposited without NH_3. At lower temperature, the C 1s peaks are broad, centered near 284.6 eV, with small shoulders near 286.0 eV. The peaks at lower BE are consistent with amorphous carbon, which is present outside of the β-WN_xC_y nanocrystals, while peaks at higher BE are ascribed to carbon in the β-WN_xC_y bonding state. This BE value is significantly higher than values reported for β-WC_x (Table I), and again is attributed to attractive N-C interaction on the interstitial sublattice of W in the β-WN_xC_y bonding state. Deconvolution (not shown) of the broad C 1s peak at 700°C in Fig. 4a yields two separate peaks, one centered at 284.8 eV and another near 286.0 eV. Interestingly, the center of the convoluted peak shifts to a slightly higher BE, due to an upward shift in BE for the deconvoluted amorphous carbon peak. This may suggest charging of the amorphous carbon at the grain boundary. The peak near 286.0 eV is much larger at 700°C relative to the lower temperatures, suggesting that carbon occupation of interstitial sites in β-WN_xC_y increases considerably above 600°C.

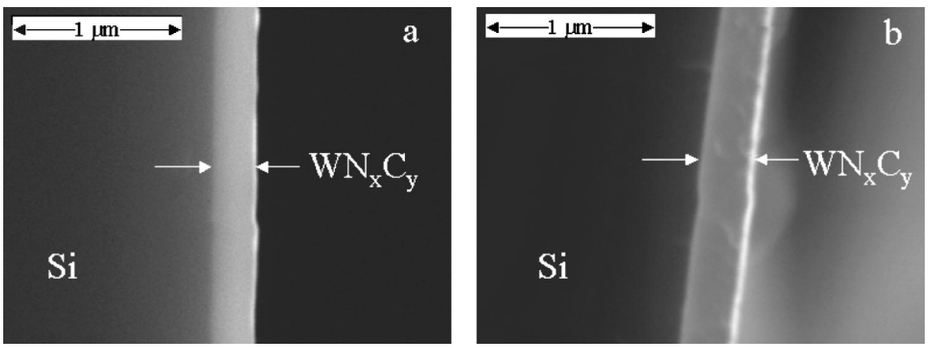

Figure 5. Cross-sectional SEM photo of films deposited with NH_3 at (a) 450 and (b) 700°C.

Figure 4c indicates that the C 1s peaks have lower intensity for films deposited with NH_3, consistent with the lower carbon content shown in Fig. 2. In addition, the convoluted peak at 700°C is narrower than that from films without NH_3, with a bump at lower BE and a small shoulder at higher BE. This suggests that NH_3 addition not only lowers the carbon content at higher temperature, but the additional nitrogen displaces carbon into the grain boundary region, leaving a smaller amount present in the β-WN_xC_y bonding state (higher BE). The additional, displaced carbon at the boundaries of the β-WN_xC_y unit cells (or nanocrystals) in the amorphous film deposited at 450°C could help to plug these regions, inhibiting oxygen indiffusion. Hence, although films deposited at 450°C with NH_3 have lower density, their microstructure may enhance resistance to oxygen intrusion in the films.

Figures 4d and b show variation of the O 1s line with deposition temperature for films deposited with and without NH_3, respectively. Oxygen levels are highest in the low-temperature films, and decrease with increasing deposition temperature due to film crystallization (which increases density) and additional carbon incorporation (which stuffs grain boundaries). The oxygen peaks for deposition without NH_3 were centered around 531.3 eV, consistent with WO_3 formation (Table I). The peaks were broad, with small shoulders at higher BE caused by WO_x, which forms during Ar^+ ion sputtering of WO_3 in the XPS chamber.[30] Similar behavior, with lower intensity, was evident for films deposited with NH_3, although the peaks are shifted to slightly higher BE, which may be due to charging effects. For deposition at 450°C, the peak intensity is noticeably lower for deposition with NH_3 than without, and is attributed to amorphous carbon stuffing boundary regions of β-WN_xC_y in the film, as discussed above.

Growth Rate

Growth rates were estimated by dividing the total film thickness (as measured by X-SEM) by deposition time. Figure 5 depicts two sample X-SEM photos. The surface of the films was smoother for those deposited with NH_3 than those without, with AFM indicating a root mean square (rms) roughness of 3.8 and 7.1 nm for films deposited at 450°C with and without NH_3, respectively. Film thickness for depositions with NH_3 varied from 2600 Å for the deposition at 450°C up to 3400 Å for deposition at 700°C. These film thicknesses correspond to deposition rates ranging from 17-23 Å/min, compared to rates of 10-27 Å/min for depositions without NH_3.[20] The growth rate of the WN_x films (as determined by X-SEM) varied with temperature, as shown in Fig. 6.

Interestingly, the deposition rate with NH_3 was enhanced at lower temperature and reduced at higher temperature relative to deposition without NH_3. In addition, deposition with NH_3 was mass transfer controlled across the entire temperature range, while deposition without NH_3 had a kinetic to mass transfer control transition point near 600°C. This indicates a shift in deposition mechanism with the addition of NH_3 as a coreactant.

Film Resistivity

Film resistivity was calculated as shown in Eq. 1

$$\rho = R_s t \quad [1]$$

where ρ is resistivity (Ω-cm), R_s is sheet resistance as measured by four-point probe (Ω/□), and t is film thickness determined by X-SEM (cm). The variation of film resistivity with deposition temperature is shown in Fig. 7, which indicates that resistivity with NH_3 goes through a maximum value of 55,000 μΩ cm at 500°C. The temperature dependence of resistivity for films deposited with NH_3 followed a trend consistent with nitrogen content, shown in Fig. 2b. Additional nitrogen in the amorphous films would increase film resistivity in two ways. First, the added nitrogen would increase resistivity in the β-WN_xC_y nanocrystals, because the resistivity is higher for β-WN_x relative to β-WC_x. Second, additional nitrogen would displace carbon from the nanocrystals to the grain boundaries. Increased amorphous carbon at the grain boundary increases electron scattering, thereby raising film resistivity. As the deposition temperature increases from 500 to 550°C, the resistivity drops sharply, caused by a decrease in nitrogen content along with film crystallization in this temperature range. A resistivity decrease is expected with decreasing nitrogen content in WN_x films.[41] At the highest temperature, resistivity for films deposited with NH_3 dropped below

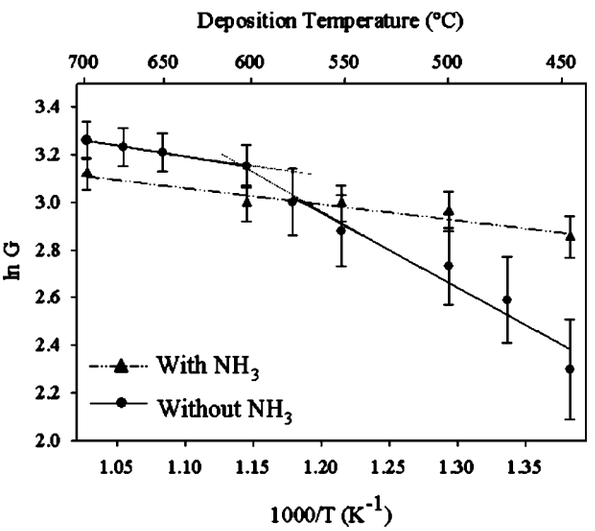

Figure 6. Dependence of film growth rate (G) on temperature for films deposited with and without NH_3. Error bars indicate uncertainty due to deposition temperature variation (±10°C) and thickness measurement from X-SEM photos.

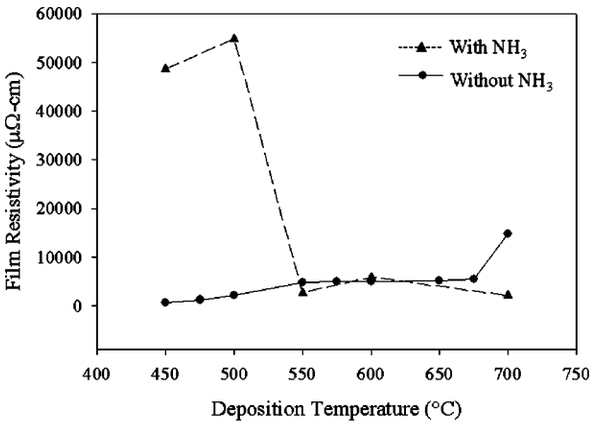

Figure 7. Film resistivity for samples grown with and without NH_3.

that for films grown without NH_3. This is due to lower carbon content, larger polycrystal grain size (not shown), and decreased thickness for films grown with NH_3.

Conclusions

Deposition of WN_x (or WN_xC_y) thin films from $Cl_4(CH_3CN)W(N^iPr)$ in the presence and absence of an NH_3 coreactant was demonstrated. AES results indicated that films grown with NH_3 had significantly higher levels of nitrogen (especially for low deposition temperatures), along with decreased levels of carbon and oxygen as compared to films grown without NH_3.

XRD and AES results suggest that increased crystallinity for films deposited at 600 and 700°C with NH_3 was due to decreased carbon content. XPS W 4f binding energies suggested the presence of W in both the β-WN_xC_y and WO_3 environments, with oxygen incorporation occurring post-growth. Moreover, due to the presence of oxygen in the films, the possibility that some $W(N, O)_x$ exists in the films cannot be ruled out, as the N 1s binding energies and XRD pattern for the oxynitride are very close to those for WN_x. While XPS indicates the presence of WO_3, XRD results do not show any WO_3 peaks. Hence, any WO_3 present in the film is likely in the form of nanocrystallites, which are not detectable by XRD. The overall film structure is amorphous at lower temperatures, and the polycrystalline films deposited at higher temperatures likely contain small WO_3 nanocrystallites embedded between larger WN_xC_y polycrystals. XPS also indicated a lack of grain boundary nitrogen in films regardless of NH_3 addition. Although some evidence of charging was apparent from the XPS results, quantification of charging through indexing of the adventitious carbon peak is difficult because the films contain carbon throughout their bulk. Adding NH_3 as a coreactant changed the mechanism for film deposition, as is reflected by the mass transfer controlled nature of film growth over the entire temperature range. Film resistivity at lower temperature was significantly higher for films deposited with NH_3, and this was attributed to additional nitrogen in β-WN_xC_y and additional carbon at the grain boundary.

To produce films appropriate for industrial barrier applications, the film thickness, resistivity, porosity, and deposition temperature must be decreased. Experiments along those lines are currently underway.

Acknowledgments

Special thanks to Eric Lambers and Bradley Willenburg of the Major Analytical Instrumentation Center (MAIC) at the University of Florida for assistance with AES/XPS and X-SEM, respectively. We thank the National Science Foundation for support under NSF-CRC grant CHE-0304810.

The University of Florida assisted in meeting the publication costs of this article.

References

1. J. Baumann, C. Kaufmann, M. Rennau, T. Werner, and T. Gessner, *Microelectron. Eng.*, **33**, 283 (1997).
2. M. Wittmer, *Appl. Phys. Lett.*, **36**, 456 (1980).
3. S. Ganguli, L. Chen, T. Levine, B. Zheng, and M. Chang, *J. Vac. Sci. Technol. B*, **18**, 237 (2000).
4. H. Li, S. Jin, H. Bender, F. Lanckmans, I. Heyvaert, K. Maex, and L. Froyen, *J. Vac. Sci. Technol. B*, **18**, 242 (2000).
5. C. H. Winter, *Aldrichim. Acta*, **33**, 3 (2000).
6. P. J. Pokela, C. K. Kwok, E. Kolawa, S. Raud, and M. A. Nicolet, *Appl. Surf. Sci.*, **53**, 364 (1991).
7. A. R. Ivanova, C. J. Galewski, C. A. Sans, T. E. Seidel, S. Grunow, K. Kumar, and A. E. Kaloyeros, in *Advanced Interconnects and Contacts*, p. 321, Materials Research Society Proceedings, Warrendale, PA (1999).
8. *Semicond. Int.*, **25**, 46 (2002).
9. M. J. Shaw, S. Grunow, and D. J. Duquette, *J. Electron. Mater.*, **30**, 1602 (2001).
10. International Technology Roadmap for Semiconductors: Interconnect. Austin, TX, International SEMATECH, 1-25 (2001).
11. C. Galewski and T. Seidel, Euro. Semicond., **1999**, 31 (Jan).
12. S. Takahashi, K. Tai, H. Ohtorii, N. Komai, Y. Segawa, H. Horikoshi, Z. Yasuda, H. Yamada, M. Ishihara, and T. Nogami, in *2002 Symposium on VLSI Technology: Digest of Technical Papers*, Honolulu, HI (2002).
13. Y. G. Shen, Y. W. Mai, W. E. McBride, Q. C. Zhang, and D. R. McKenzie, *Thin Solid Films*, **372**, 257 (2000).
14. J. E. Kelsey, C. Goldberg, G. Nuesca, G. Peterson, A. E. Kaloyeros, and B. Arkles, *J. Vac. Sci. Technol. B*, **17**, 1101 (1999).
15. R. G. Gordon, S. Barry, R. N. R. Broomhall-Dillard, V. A. Wagner, and Y. Wang, *Mater. Res. Soc. Symp. Proc.*, **612**, 9.12/1 (2000).
16. H. T. Chiu and S. H. Chuang, *Mater. Res.*, **8**, 1353 (1993).
17. M. H. Tsai, S. C. Sun, H. T. Chiu, and S. H. Chuang, *Appl. Phys. Lett.*, **68**, 1412 (1996).
18. J. S. Becker, S. Suh, S. Wang, and R. G. Gordon, *Chem. Mater.*, **15**, 2969 (2003).
19. S. W. Johnston, C. G. Ortiz, O. J. Bchir, Y. Zhang, L. McElwee-White, and T. J. Anderson, in *Chemical Vapor Deposition: CVD XV*, M. D. Allendorf and T. M. Besmann, Editors, PV 2000-13, p. 268, The Electrochemical Society Proceedings Series, Pennington, NJ (2000).
20. O. J. Bchir, S. W. Johnston, A. C. Cuadra, T. J. Anderson, C. G. Ortiz, B. C. Brooks, D. H. Powell, and L. McElwee-White, *J. Cryst. Growth*, **249**, 262 (2003).
21. C. J. Galewski, P. N. Gadgil, L. D. Matthysse, C. A. Sans, and V. S. Dharmadhikari, in *ULSI XII*, p. 277, MRS, Warrendale, PA (1997).
22. O. J. Bchir, K. M. Green, M. S. Hlad, T. J. Anderson, B. C. Brooks, C. B. Wilder, D. H. Powell, and L. McElwee-White, *J. Organomet. Chem.*, **684**, 338 (2003).
23. Powder Diffraction File 25-1257. JCPDS, International Center for Diffraction Data, Swarthmore, PA (1988).
24. Powder Diffraction File 20-1316. JCPDS, International Center for Diffraction Data, Swarthmore, PA (1988).
25. S. J. Wang, H. Y. Tsai, S. C. Sun, and M. H. Shiao, *J. Electrochem. Soc.*, **148**, G500 (2001).
26. H. P. Kattelus, E. Kolawa, K. Affolter, and M. A. Nicolet, *J. Vac. Sci. Technol. A*, **3**, 2246 (1985).
27. S. D. Marcus and R. F. Foster, *Thin Solid Films*, **236**, 330 (1993).
28. S. H. Kim, D. S. Chung, K. C. Park, K. B. Kim, and S. H. Min, *J. Electrochem. Soc.*, **146**, 1455 (1999).
29. R. J. Colton and J. W. Rabalais, *Inorg. Chem.*, **15**, 236 (1976).
30. H. L. Zhang, D. Z. Wang, and N. K. Huang, *Appl. Surf. Sci.*, **150**, 34 (1999).
31. Y. G. Shen and Y. W. Mai, *Mater. Sci. Eng., A*, **288**, 47 (2000).
32. J. S. Lee, C. S. Park, J. Y. Kang, D. S. Ma, and J. Y. Lee, *J. Vac. Sci. Technol. B*, **8**, 1117 (1990).
33. M. Nagai and K. Kishida, *Appl. Surf. Sci.*, **70**, 759 (1993).
34. T. Nakajima, K. Watanabe, and N. Watanabe, *J. Electrochem. Soc.*, **134**, 3175 (1987).
35. P. J. C. Chappell, M. H. Kibel, and B. G. Baker, *J. Catal.*, **110**, 139 (1988).
36. G. Leclercq, M. Kamal, J. M. Giraudon, P. Devassine, L. Feigenbaum, L. Leclercq, A. Frennet, J. M. Bastin, A. Lofberg, S. Decker, and M. Dufour, *J. Catal.*, **158**, 142 (1996).
37. V. Crist, *Handbook of Monochromatic XPS Spectra: The Elements and Native Oxides*, John Wiley & Sons, New York (2000).
38. J. Luthin and C. Linsmeier, *J. Nucl. Mater.*, **290-293**, 121 (2001).
39. Powder Diffraction File 25-1255. JCPDS, International Center for Diffraction Data, Swarthmore, PA (1982,1988).
40. B.-J. Lee, *Metall. Mater. Trans. A*, **32**, 2423 (2001).
41. C. W. Lee, Y. T. Kim, and S. K. Min, *Appl. Phys. Lett.*, **62**, 3312 (1993).